Journal of Magnetism and Magnetic Materials 514 (2020) 167152

Contents lists available at ScienceDirect

Journal of Magnetism and Magnetic Materials

journal homepage: www.elsevier.com/locate/jmmm

Research articles

Magnetic properties and magnetic structures of R_2PdGe_6 (R = Pr, Nd, Gd-Er) and R_2PtGe_6 (R = Tb, Ho, Er)

Bogusław Penc[a], Stanisław Baran[a,*], Andreas Hoser[b], Janusz Przewoźnik[c], Andrzej Szytuła[a]

[a] M. Smoluchowski Institute of Physics, Jagiellonian University, Łojasiewicza 11, 30-348, Kraków, Poland
[b] Helmholtz-Zentrum Berlin für Materialien und Energie GmbH, Hahn-Meitner Platz 1, D-14109 Berlin, Germany
[c] AGH University of Science and Technology, Faculty of Physics and Applied Computer Science, Department of Solid State Physics, Al. Mickiewicza 30, 30-059 Kraków, Poland

ARTICLE INFO

Keywords:
Rare earth intermetallics
Germanides
Magnetic properties
Magnetic structure
Neutron diffraction
Specific heat

ABSTRACT

Polycrystalline samples of the intermetallic compounds R_2PdGe_6 (R = Pr, Nd, Gd-Er) and R_2PtGe_6 (R = Tb, Ho, Er) have been studied using X-ray diffraction as well as magnetometric and neutron diffraction measurements. All compounds have an orthorhombic crystal structure of the Yb_2PdGe_6-type (space group *Cmca*) and are antiferromagnetic with the Néel temperatures ranging from 4.9 K for Er_2PtGe_6 up to 48 K for Tb_2PdGe_6. The magnetic properties and specific heat data collected for Nd_2PdGe_6 show the presence of an additional phase transition below T_N at T = 4 K. Based on the neutron diffraction data, the magnetic structures have been determined for R_2PdGe_6 (R = Pr, Nd, Tb, Dy, Ho) and R_2PtGe_6 (R = Tb and Er). Both the magnetic properties and neutron diffraction data indicate that the magnetic moment is localized on rare earth atoms. The magnetic unit cell is equal to the crystal one, however, individual compounds show different types of magnetic orderings. Magnetic moments in Pr_2PdGe_6 form a non-collinear antiferromagnetic structure at low temperatures with magnetic moments confined to the (001) plane. The low temperature magnetic structure in Nd_2PdGe_6 is a collinear antiferromagnetic one with moments parallel to the b-axis and coupled ferromagnetically within the (001) plane, while along the c-axis the moments follow the + − − + sequence. With increasing temperature, a transition to a modulated magnetic structure is observed in Nd_2PdGe_6 at T = 4 K. The magnetic moments in R_2PdGe_6 (R = Tb, Dy, Ho) and Tb_2PtGe_6 assume a non-collinear antiferromagnetic order within the (001) plane with the + − + − sequence of signs of the moments in the neighboring planes along the c-axis. The Er moments in Er_2PtGe_6 form a collinear magnetic structure with magnetic moments oriented along the a-axis and coupled ferromagnetically within the (001) plane. Along the c-axis the moments follow the + − + − sequence. The magnetic structures determined here are discussed on the basis of the competition between the RKKY-type interactions and influence of Crystalline Electric Field.

1. Introduction

Ternary intermetallics composed of rare-earth elements, transition d-metals and p-electron elements attract special attention mainly due to a wide variety of chemical composition, crystal structure and interesting magnetic properties. One of the most interesting groups are ternary compounds of a general formula R_2TGe_6, where R is a rare earth element and T is a d-transition element. These compounds, originally synthesized with T = Cu, crystallize in an orthorhombic crystal structure of the Ce_2CuGe_6-type (space group *Amm*2, No. 38) [1]. The same type of a crystal structure was later found for the compounds with T = Pd, Pt, Ag, Au [2]. More recent single crystal data for R_2TGe_6 (R = Y, Ce, Pr, Nd, Dy, Er, Yb and Lu; T = Pd, Pt) suggest a new type of an orthorhombic crystal structure with lattice parameters: 2a, 2b and c with respect to the previous model, and the *Cmca* space group (No. 64) [3–7].

Magnetic data have been collected for the R_2NiGe_6 and R_2CuGe_6 compounds with R = Ce, Pr, Nd, Gd-Tm. These compounds are antiferromagnets at low temperatures [2,8–11]. For some of them also their magnetic structures have been determined [12–15]. The magnetic moments are found to be localized exclusively on the rare-earth elements. For Nd_2TGe_6 (T = Ni and Cu) and R_2NiGe_6 (R = Tb, Ho and Er) they form a simple collinear magnetic structure with the magnetic unit cell identical to the crystal one while R_2CuGe_6 (R = Ho and Er) have a magnetic unit cell doubled along the a-axis. Temperature dependence of the electrical resistivity indicates a metallic behavior of R_2TGe_6

* Corresponding author.
E-mail address: stanislaw.baran@uj.edu.pl (S. Baran).

https://doi.org/10.1016/j.jmmm.2020.167152
Received 5 March 2020; Received in revised form 8 June 2020; Accepted 14 June 2020
Available online 18 June 2020

(T = Mn, Ni, Cu) [16,17].

Magnetic properties have been reported for only a few Pd- and Pt-based compounds. The R_2PdGe_6 compounds are antiferromagnets with the Néel temperatures equal to 11.5 K (Ce) [2,18,19], 14 K (Pr) [20,21], 30 K (Sm) [22], 34 K (Gd) and 48 K (Tb) [21] and 25 K (Dy) [6]. La_2PdGe_6 is a Pauli paramagnet [6], while Yb_2PdGe_6 is an intermediate valence material with a highly unstable 4f shell of the Yb ions [5,22]. Also some of the R_2PtGe_6 compounds are antiferromagnets with the Néel temperature equal to 9.9 K (Ce) [18] and 23 K (Sm) [22]. Yb_2TGe_6 (T = Pd and Pt) have been found to be Pauli paramagnets [23].

In order to investigate the influence of the T element on the magnetic properties, including the magnetic order, we have performed a systematic investigation of the polycrystalline samples of selected compounds with T = Pd and Pt by measuring DC magnetic susceptibility and magnetization as well as performing neutron diffraction experiments. Out of these data, information has been extracted on the crystal structure and on the dependence of magnetic properties, including magnetic structures, on temperature.

2. Experiment

Large samples of R_2PdGe_6 (R = Pr, Nd, Gd-Er) and R_2PtGe_6 (R = Tb, Ho, Er) (~5 g each) were prepared by arc melting of pure elements taken in stoichiometric ratio (element purity: 3 N for all R, 4 N for Pd and Pt and 5 N for Ge). The samples were annealed at 870 K in evacuated quartz tubes for one week and then quenched in cold water.

The quality of the samples was checked by X-ray powder diffraction at room temperature with Cu K_α radiation on X'Pert PRO X-ray diffractometer.

Magnetic measurements were performed in the temperature range 1.9–390 K on a vibrating sample magnetometer (VSM) option of the Physical Property Measurement System (PPMS) by Quantum Design. DC magnetic susceptibility measurements were carried out in applied magnetic fields of 50 Oe and 1 kOe while isothermal hysteresis loops were collected at T = 1.9 K in the external magnetic fields up to 90 kOe.

For the Nd_2PdGe_6 compound an additional heat capacity study was carried out by a two-tau relaxation method in the temperature range 2–114 K.

Neutron diffraction patterns were collected at different temperatures using the wavelength of λ = 2.4315 Å on the E6 diffractometer (BER II reactor, BENSC, Helmholtz-Zentrum-Berlin). The Rietveld-type program FullProf [24] was used for processing the diffraction data.

3. Results

All investigted compounds have similar X-ray diffraction pattern at room temperature. The patterns for Tb_2TGe_6 (T = Pd, Pt) have been choosen as representatives and are shown in Fig. 1. Numerical analysis of the X-ray diffraction data has been performed for models of the crystal structure related to both the *Amm*2 and *Cmca* space groups, as mentioned in the Introduction section. Considerably lower values of the reliability factors clearly favor the model with the *Cmca* space group, except the Ho_2PtGe_6 sample where both structure types lead to comparable values of the reliability fators (see Table 1). Validity of the selected crystal structure model is further confirmed by the presence in the X-ray diffraction pattern of the Bragg peaks at 2θ = 16.0°, 17.6°, 19.8°, 29.3°, 35.5°, 36.0° and 37.2° (see Fig. 1a), which are expected for a structure of the Ce_2CuGe_6-type. A detailed analysis of the crystal structure is present in the section 3.3.1 together with the neutron diffraction data.

3.1. Magnetic data

The temperature dependence of the reciprocal magnetic susceptibilities is displayed in Fig. 2a–j. In a broad temperature range a linear

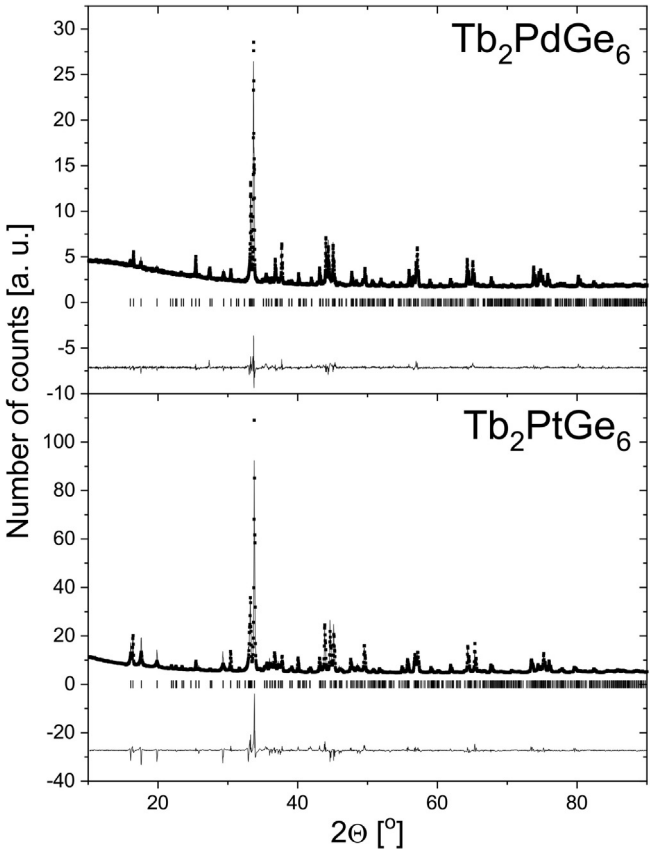

Fig. 1. X-ray (Cu K_α, λ = 1.5418 Å) powder diffraction patterns of the Tb_2TGe_6 (T = Pd, Pt) compounds, collected at room temperature. The squares represent the experimental points. The solid lines indicate the calculated profile of the crystal structure and the difference between the obtained and calculated intensity (in the bottom of diagram). The vertical bars indicate positions of Bragg reflections.

Table 1
The values of the R_{Bragg} and R_{prof} reliability factors for selected R_2TGe_6 (T = Pd, Pt) compounds for two different models of the crystal structure described by the *Amm*2 and *Cmca* space group, respectively. These were obtained from the refinement of the X-ray data taken at room temperature and neutron diffraction data taken at low temperatures in the paramagnetic state.

Compound	Method	R_{Bragg} [%]		R_{prof} [%]	
		*Amm*2	*Cmca*	*Amm*2	*Cmca*
Pr_2PdGe_6	XRD	20.3	11.8	5.44	3.71
Pr_2PdGe_6	ND	16.1	6.67	11.3	5.27
Nd_2PdGe_6	XRD	18.2	10.7	4.69	3.39
Nd_2PdGe_6	ND	14.7	5.59	8.30	3.39
Gd_2PdGe_6	XRD	19.1	12.0	3.31	2.44
Tb_2PdGe_6	XRD	19.9	10.4	3.72	2.57
Tb_2PdGe_6	ND	14.5	8.80	7.39	4.61
Dy_2PdGe_6	XRD	18.3	11.8	3.15	2.34
Dy_2PdGe_6	ND	10.3	7.56	2.77	2.34
Ho_2PdGe_6	XRD	21.3	14.1	5.97	4.10
Ho_2PdGe_6	ND	10.3	6.22	4.15	2.70
Er_2PdGe_6	XRD	17.3	12.6	5.55	4.15
Tb_2PtGe_6	XRD	24.7	12.7	6.31	4.24
Tb_2PtGe_6	ND	12.9	4.91	5.90	2.72
Ho_2PtGe_6	XRD	21.9	22.7	6.01	6.38
Er_2PtGe_6	XRD	17.6	18.6	9.92	9.46
Er_2PtGe_6	ND	11.4	9.21	5.37	5.14

dependence is observed, described by the Curie-Weiss formula: $\chi(T) = C/(T - \Theta_p)$. In this equation C refers to a Curie constant, which is related to the effective magnetic moment by formula $\mu_{eff} = (8C)^{1/2}$,

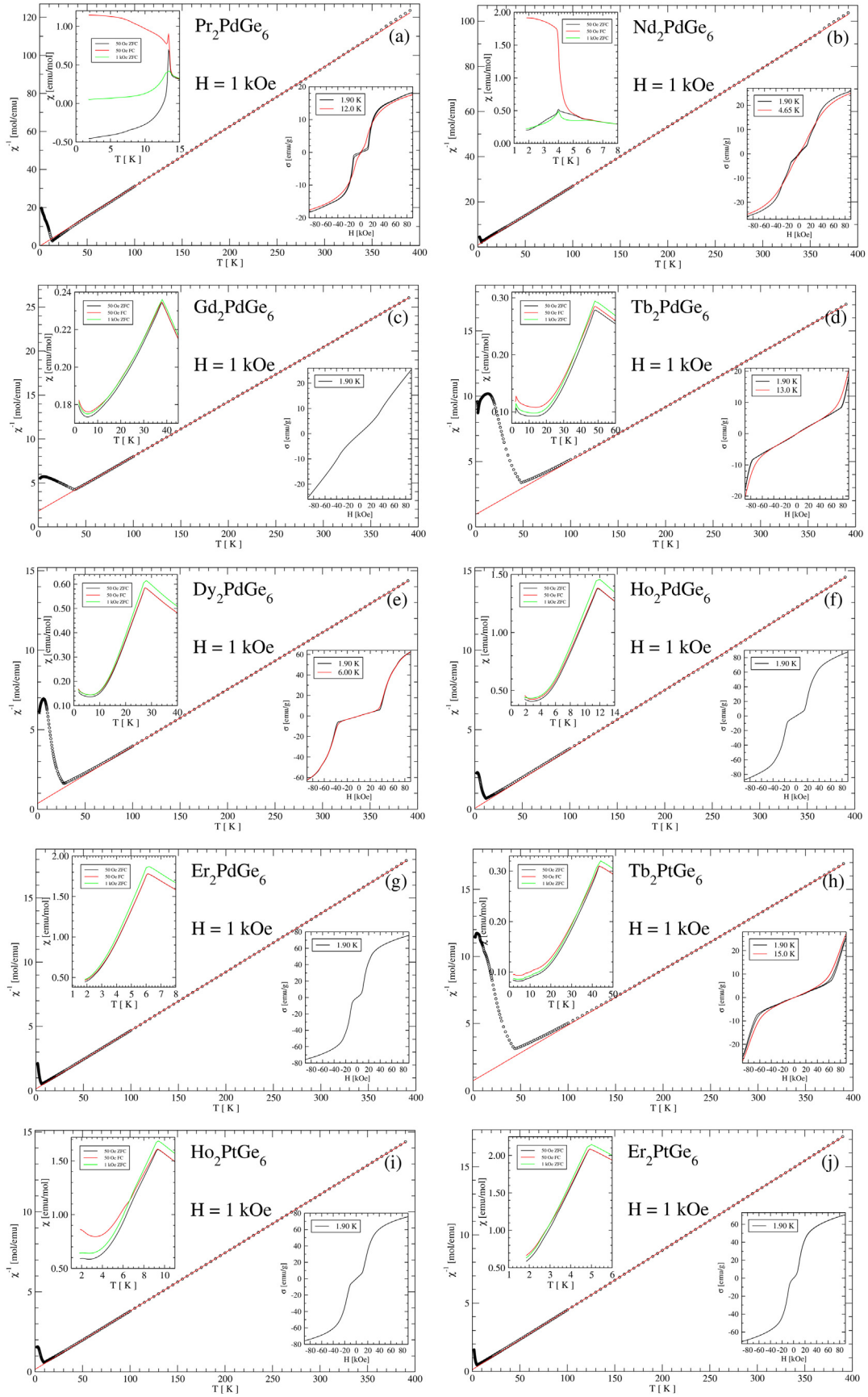

Fig. 2. Temperature dependence of the reciprocal magnetic susceptibility of a) Pr_2PdGe_6, b) Nd_2PdGe_6, c) Gd_2PdGe_6, d) Tb_2PdGe_6, e) Dy_2PdGe_6, f) Ho_2PdGe_6, g) Er_2PdGe_6, h) Tb_2PtGe_6, i) Ho_2PtGe_6 and j) Er_2PtGe_6 measured at the external magnetic field of 1 kOe. The insets: the upper ones – temperature dependence of the magnetic susceptibility at low temperatures taken at 50 Oe (ZFC and FC) and at 1 kOe (ZFC); the lower ones – hysteresis loop between −90 kOe and 90 kOe at T = 1.9 K.

Table 2
Magnetic data for the R_2TGe_6 (T = Pd, Pt) compounds. T_N refers to the Néel temperature; Θ_p is the paramagnetic Curie temperature; μ_{eff} is the effective magnetic moment; μ_s is the moment at T = 1.9 K and H = 90 kOe determined by magnetization measurements (M) and by neutron diffraction at the lowest temperature (ND); next to the experimental (exp), the theoretical (theor) values are shown for reference. H_{cr} is the critical magnetic field from magnetometric measurements and DMM is the direction of the magnetic moment as determined from neutron diffraction. R_{magn} is the magnetic reliability factor.

R	T_N [K]	Θ_p [K]	μ_{eff} [μ_B]		μ_s [μ_B]			H_{cr} [kOe]	DMM	R_{magn} [%]	Ref.
			exp	theor	exp M	exp ND	theor				
R_2PdGe_6											
Ce	11.5	−16	2.52	2.54	0.90		2.14	11			[2,18,19]
Pr	13	+1.1	3.56	3.58	1.35	2.82(5)	3.20	14	in plane a-b	9.4	this work
Nd	6.5	−3.5	3.60	3.62	1.91	2.11(2)	3.27	16, 31	||b	7.3	this work
Sm	30	−11.6									[22]
Gd	38	−29	8.01	7.92	1.95		7.00	35	||b		this work
Tb	48	−23	9.85	9.72	1.60	8.64(7)	9.00	> 90	in plane a-b	5.4	this work
Dy	28	−10.1	10.56	10.65	4.87	7.80(8)	10.00	43	in plane a-b	8.6	this work
Ho	11.8	−1.4	10.36	10.61	6.86	8.39(7)	10.00	19	in plane a-b	6.4	this work
Er	6.2	−3.1	9.37	9.58	5.94		9.00	11			this work
R_2PtGe_6											
Ce	9.9	−7.0	2.43	2.54	1.82		2.14	1.1			[18]
Sm	23	−10.8									[22]
Tb	44	−18	9.83	9.72	2.18	8.86(6)	9.00	82	in plane a-b	2.7	this work
Ho	9.5	−4.2	10.47	10.61	6.52		10.00	16			this work
Er	4.9	−2.8	9.56	9.58	6.10	7.58(9)	9.00	10	||a	6.9	this work

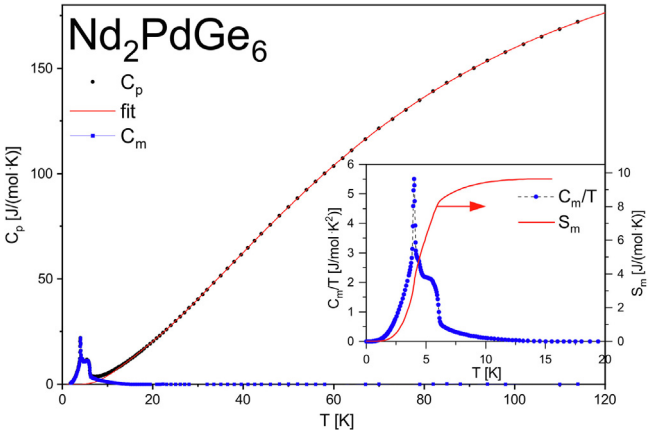

Fig 3. Temperature dependence of the specific heat of Nd_2PdGe_6 in the temperature range of 2–114 K. The solid line represents the phononic contribution, as discussed in the text. The inset presents the low temperature part of the C_m/T (dots) and magnetic entropy S_m (solid line).

Table 3
The Debye (Θ_D) and Einstein (Θ_{Ei}) temperatures together with the anharmonic coefficient (α). These were obtained from the fitting of the formula describing phononic contribution to the C_p vs. T dependence for Nd_2PdGe_6 (see Fig. 3). m_i denotes multiplicities of the Θ_{Ei} parameters.

Parameter	Value	m_i
Debye temperature Θ_D [K]	145(5)	
Einstein temperatures: Θ_{E1} [K]	53.6(7)	3
Θ_{E2} [K]	158(2)	9
Θ_{E3} [K]	270(13)	4
Θ_{E4} [K]	314(7)	8
Anharmonic coefficient α [1/K]	$1.37(15)\cdot10^{-4}$	

while Θ_p is a paramagnetic Curie temperature. The least squares fitting of the experimental data gave values of the effective magnetic moments and the paramagnetic Curie temperatures which are listed in Table 2. The values of μ_{eff} are close to those predicted for free R^{3+} ions. The paramagnetic Curie temperatures, except the one for R = Pr, are negative, indicating dominant character of antiferromagnetic interactions. This result is in agreement with the maxima observed at low temperatures in the temperature dependence of magnetic susceptibilities (see insets in Fig. 2a–j), which are typical of antiferro- to paramagnetic transition. The Néel temperatures determined be the measurement are listed in Table 2. For the Tb-based compounds an additional small intensity maximum, related to the Tb_2O_3 impurity phase, is visible at 2.4 K. For R = Nd, a jump at T = 4 K indicates the presence of an additional magnetic phase transition. Hysteresis loops taken at 1.9 K confirm antiferromagnetic properties and show a metamagnetic phase transition. The values of the critical fields connected with the metamagnetic phase transition are listed in Table 2.

3.2. Specific heat data

Fig. 3 presents the temperature dependence of the Nd_2PdGe_6 specific heat in the temperature range of 2–114 K. A high temperature part of the specific heat dependence, i.e. the one above 15.5 K, was analyzed in terms of the following formula:

$$C_p = C_{ph+el} = \frac{9R}{1-\alpha T}\left(\frac{T}{\theta_D}\right)^3 \int_0^{\frac{\theta_D}{T}} \frac{x^4 e^x}{(e^x-1)^2}dx + \frac{R}{1-\alpha T}\sum_i m_i \frac{\left(\frac{\theta_{Ei}}{T}\right)^2 \exp\left(\frac{\theta_{Ei}}{T}\right)}{\left(\exp\left(\frac{\theta_{Ei}}{T}\right)-1\right)^2}$$

where Θ_D is a Debye temperature, Θ_{Ei} are Einstein temperatures and m_i are corresponding multiplicities for each individual optical branch. α stands for an anharmonic coefficient and R is the gas constant. The electronic contribution to the specific heat – usually introduced as γT, where γ is an electronic specific heat (Sommerfeld) coefficient – is omitted as the values of γ reported for the isostructural R_2PdGe_6 compounds are small: 3.6 mJ/(mol·K^2) (R = La) [6] and 14 mJ/(mol·K^2) (R = Ce) [19] and therefore this term can be neglected at higher temperatures where the phononic contribution is dominant. With nine atoms per molecule of Nd_2PdGe_6, there are in total 3x9 = 27 phonon modes: 3 acoustic and 24 optical ones. In order to facilitate analysis, the summation over 24 independent optical branches was grouped into 4 branches with the 3, 9, 4, 8-fold multiplicities. A fit to the experimental data (denoted in Fig. 3 by a red solid line) was performed from 15.5 K to 114 K, i.e. far above the peaks observed at low temperatures. The corresponding fit parameters are gathered in Table 3.

The low temperature data of the Nd_2PdGe_6 specific heat reveal a complex behavior with a sharp maximum at T = 4 K (see also the C_m/T data in the inset of Fig. 3) hinting at its first order character. This is in

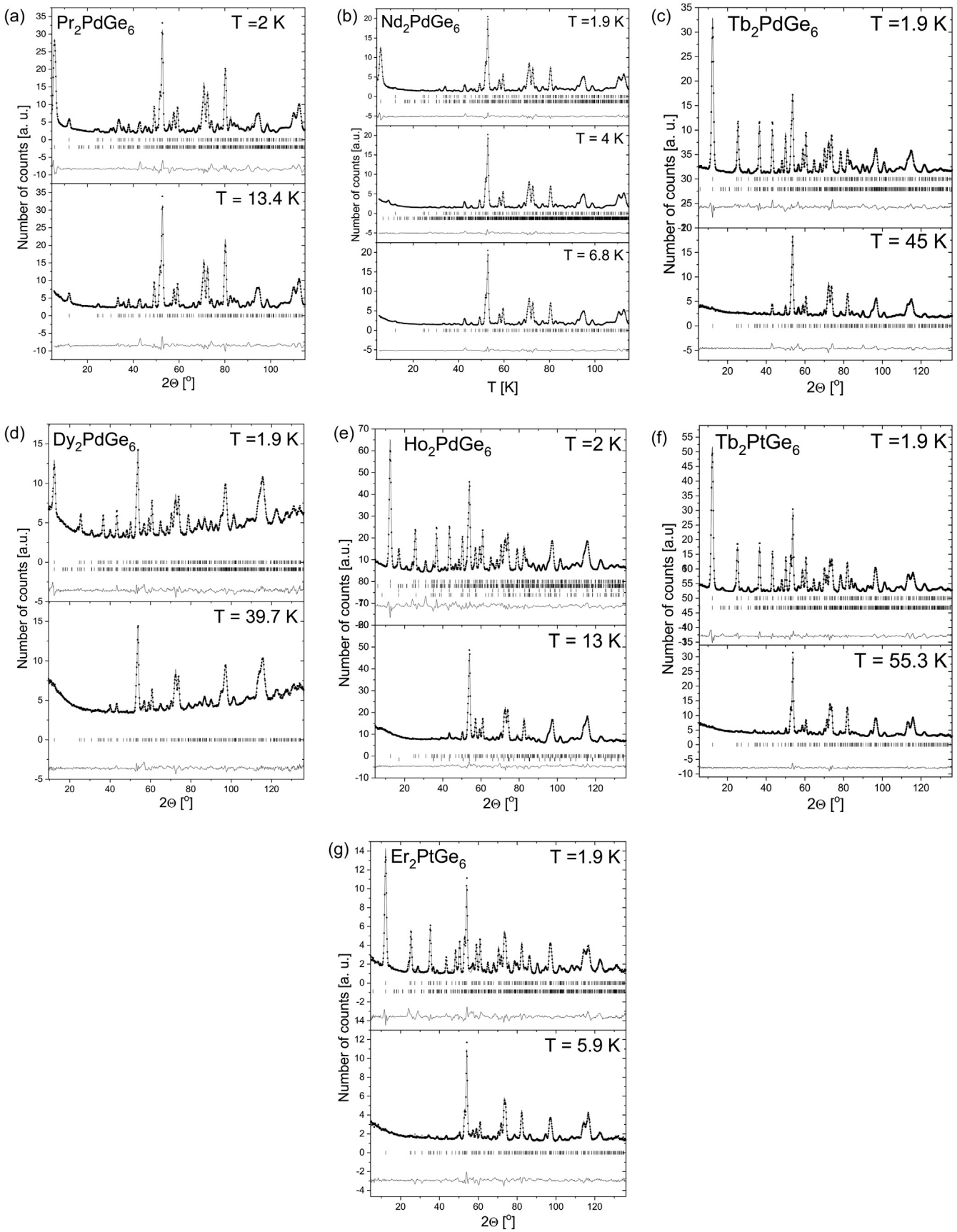

Fig. 4. Neutron diffraction patterns of a) Pr_2PdGe_6 at 2.0 and 13.4 K, b) Nd_2PdGe_6 at 1.9, 4.0 and 6.8 K, c) Tb_2PdGe_6 at 1.9 and 60.4 K, d) Dy_2PdGe_6 at 1.9 and 39.7 K, e) Ho_2PdGe_6 at 1.9 and 13 K, f) Tb_2PtGe_6 at 1.9 and 55.3 K) and g) Er_2PtGe_6 at 1.9 and 5.9 K. The squares represent the experimental points. The solid lines indicate the calculated profile of the crystal structure and the difference between the obtained and calculated intensity (in the bottom of the diagram). The vertical bars indicate the positions of Bragg reflections: nuclear (first row) and magnetic (second row) ones. The diffraction patterns of Ho_2PdGe_6 (the inset e) contain a small contribution originating from $HoPd_{0.22}Ge_2$. The third and fourth rows of the vertical bars refer to the nuclear and magnetic contributions arising from $HoPd_{0.22}Ge_2$.

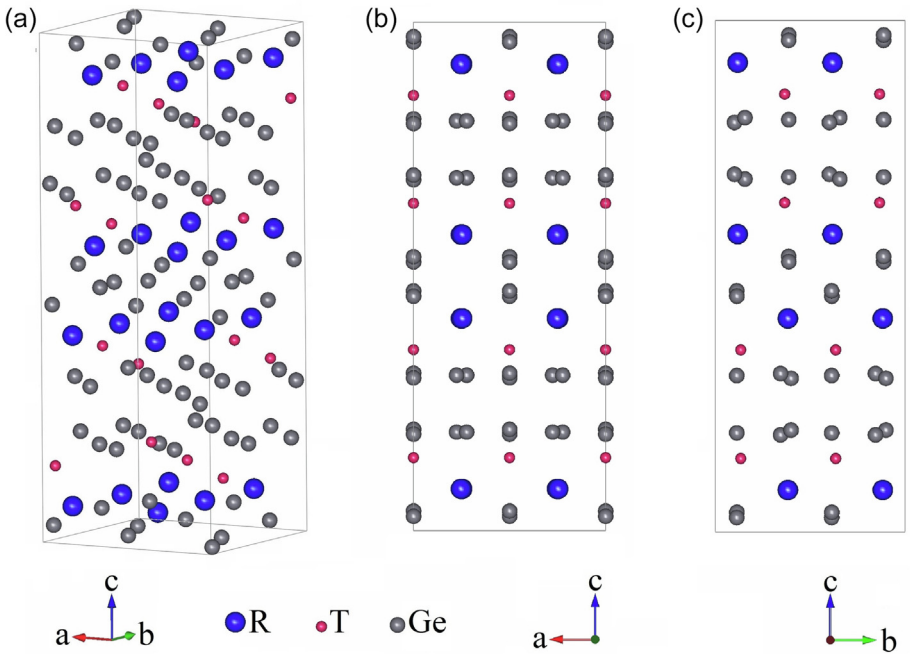

Fig. 5. Crystal structure of the R_2TGe_6 (T = Pd, Pt) compounds: a) orthorhombic crystal unit cell together with projection on the b) a-c and c) b-c planes.

agreement with the DC magnetic data (see the inset in Fig. 2b). With increasing temperature a small maximum at T = 4.2 K followed by a broad one at T = 5.6 K with a quick decrease at 6 K are observed. These anomalies corelate with a small maximum in the magnetic susceptibility visible at 6.5 K (see Fig. 2b).

The Nd^{3+} ions occupy the 16 g crystallographic position in the crystal unit cell of Nd_2PdGe_6. The crystal field potential of the symmetry related to the 16 g Wyckoff site splits the neodymium $^4I_{9/2}$ ground multiptet into five doublets. The temperature variation of the magnetic entropy $S_m(T)$ derived from the C_m/T dependence (see the inset in Fig. 3) exhibits a distinct change in slope at the Néel temperature. $S_m(T)$ above T_N reaches the value of 9.64 J/(mol·K^2) which is in reasonable agreement with the theoretical one of 2Rln2 = 11.53 J/(mol·K^2) expected for the doublet ground state of $2N_A$ Nd^{3+} ions within one mole of Nd_2PdGe_6 (N_A is the Avogadro number). A discrepancy between these two numbers can be attributed to a systematic error related to the estimation of the phononic contribution to the specific heat which was subtracted from the experimental data in order to obtain the pure magnetic contribution.

3.3. Neutron diffraction data

3.3.1. Crystal structure

The neutron difraction patterns in the paramagnetic state, collected above the respective Néel temperatures (see Fig. 4a–g), confirm that all samples have an orthorhombic crystal structure of the Yb_2PdGe_6-type [3]. In the unit cell of this structure the atoms occupy the following positions: the R and Ge1 atoms at the 16 g sites: (x, y, z) while the Pd or Pt atoms as well as Ge2, Ge3, Ge4 and Ge5 atoms at the 8f sites: (0, y, z) with different values of x_i, y_i, and z_i for each corresponding atom. The values of the lattice parameters and atomic positional parameters determined here are listed in Table 3. This type of a crystal structure is characterized by a sequence of atomic planes stacked along a much-elongated c-axis (c/(a,b) ~ 2.65) with the values of a and b lattice parameters very close one to another (a/b ~ 1.015) resulting in a layered structure with large distances between the magnetic rare-earth atoms (see Fig. 5).

3.3.2. Magnetic structure

All the neutron diffraction patterns collected for the samples below their respective Néel temperatures contain a large numer of additional peaks of the magnetic origin (see Fig. 4a–g) which can be indexed within a magnetic unit cell identical with the crystal one, suggesting that the magnetic structure is a commensurate one with the propagation vector **k** = [0, 0, 0]. A high-intensity peak at 2Θ = 6.3° observed for R_2PdGe_6 (R = Pr, Nd) and indexed as (0 0 1) as well as the one at 2Θ = 12.7° indexed as (0 0 2) and found for all the other compounds imply that the magnetic moments lay in the basal a-b plane. The 16 rare-earth atoms in the unit cell occupy the 16 g Wyckoff site (with coordinates of particular rare earth atoms listed in Table 5). In order to determine magnetic structures, a symmetry analysis has been performed for the R moments occupying the 16 g Wyckoff site. The basireps computer program, which is distributed together with FullProf [24], was utilized for the symmetry analysis. Naming of the rare earth ions positions as well as irreducible representations follows the nomenclature introduced by Qi et al. [15]. The full symmetry analysis is presented in Table 1 in Ref. [15]. In this work only the magnetic structure models that fit the experimental data are described in details. In the text below, the u parameter refers to the x-component of the Fourier coefficient of the magnetic moment, and the v parameter to the y- component thereof.

The magnetic order in Pr_2PdGe_6 is found to be a non-collinear antiferromagnetic one with magnetic moments consisting of the components along the a- and b-axes, related to the $\Gamma_3(u)$ and $\Gamma_3(v)$ models, respectively (see Table 5). The a-axis component of the Pr magnetic moment is equal to 1.42(8) μ_B while the b-axis one to 2.43(3) μ_B, resulting in a total moment of 2.82(5) μ_B at 2.0 K (R_{magn} = 9.2%). This order is stable up to the Néel temperature of 13 K.

A similar magnetic structure model is found in Nd_2PdGe_6 except the fact that only the b-axis magnetic moment component, related to $\Gamma_3(v)$, is present (see Fig. 6b). This magnetic order is stable within the temperature range 1.5 K–3.5 K. The Nd magnetic moment equals 2.11(2) μ_B at 1.5 K (R_{magn} = 7.3%). A transition to a modulated magnetic structure related to the propagation vector **k** = [0.333, 0.27, 0] takes place around 4 K (see Fig. 6c).

The powder diffraction patterns of R_2PdGe_6 (R = Tb, Dy and Ho) and Tb_2PtGe_6 collected at low temperatures show similar distribution of

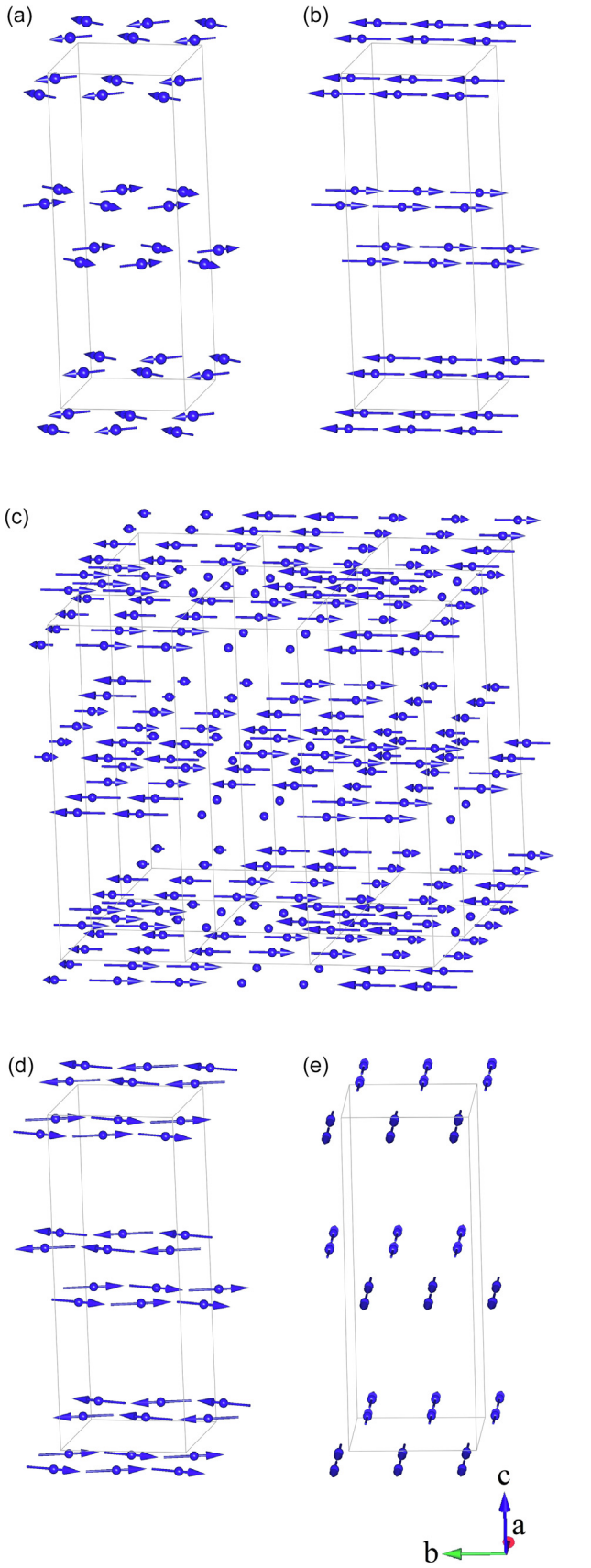

Fig. 6. Magnetic structures of a) Pr_2PdGe_6, b) Nd_2PdGe_6 (the low temperature phase), c) Nd_2PdGe_6 (the high temperature phase), d) R_2PdGe_6 (R = Tb, Dy Ho) and Tb_2PtGe_6, and e) Er_2PdGe_6,

magnetic reflections. A detailed analysis of the magnetic contribution to the patterns indicate that:

- the high-intensity reflections correspond to the magnetic order related to the Γ_8(v) model (see Table 4) with magnetic moments along the b-axis and magnitudes of 8.32(7), 7.04(8), 7.42(7) and 8.50(5) μ_B, respectively,
- the low-intensity reflections correspond to the magnetic order related to the Γ_8(u) model with magnetic moments along the a-axis and magnitudes of 2.29(7), 3.39(7), 3.39(3) and 2.27(7) μ_B, respectively.

As a result, a non-collinear magnetic structure is developed (see Fig. 6d) with the total magnetic moments equal to 8.64(7), 7.80(8), 8.39(7) and 8.86(6) μ_B, respectively, and the corresponding values of the R_{magn} factor of 5.4, 8.6, 6.4 and 2.7%. This order is stable up to the Néel temperature.

A different distribution of the peaks of the magnetic origin is observed in Er_2PtGe_6. The Bragg reflections of the magnetic origin can be indexed in the magnetic unit cell identical with the crystal one (**k** = [0, 0, 0]). Analysis of the intensity of magnetic reflections shows that the magnetic ordering of Er moments corresponds to the Γ_6(u) model (see Table 5) with the moment equal to 7.58(9) μ_B (at 1.9 K) and parallel to the a-axis (see Fig. 6e) (R_{magn} = 6.9%). This order is stable up to the Néel temperature.

The values of the magnetic moments derived from neutron diffraction data are listed in Table 2.

3.3.3. Temperature dependence of the parameters of the crystal and magnetic structures

For all the compounds the neutron diffraction patterns have been collected as a function of temperature. Based on these data, the temperature dependences of the a, b, c lattice parameters, unit cell volume and values of the magnetic moments have been determined and are presented in Fig. 7. In all of the compounds, except Nd_2PdGe_6, the low temperature magnetic structures are stable up to the respective Néel temperatures. The transition between the antiferro- and paramagnetic states is associated with a jump in the lattice parameters and unit cell volume. In the case of Nd_2PdGe_6, this effect is found only for the transition between the commensurate collinear antiferromagnetic ordering and the incommensurate modulated one which takes place around 4 K. For this compound no further change in lattice parameters and unit cell volume is detected at the Néel temperature. The numerical values of the changes in the lattice parameters and unit cell volume together with the magnetic moments derived from neutron diffraction data are summarized in Table 6. One can find that the jumps in the lattice parameters are relatively large for the R_2PtGe_6 compounds.

4. Discussion

The results of the X-ray and neutron diffraction measurements presented in this work confirm that the investigated compounds have an orthorhombic crystal structure of the Yb_2PdGe_6-type. Magnetic measurements and neutron diffraction data indicate that the compounds are antiferromagnets with the magnetic moments localized on the rare-earth atoms. The determined values of the effective magnetic moments are close to those predicted for free R^{3+} ions while the magnetic moments in the ordered state, as found from magnetization as well as from the neutron diffraction data, are smaller than those of free R^{3+} ions.

The layered magnetic structures determined for the R_2TGe_6 (T = Pd, Pt) compounds are characterized by a ferromagnetic or nearly ferromagnetic arrangement of the R moments within the (0 0 1) plane and two different sequences of the moments in the neighboring planes, i.e. along the c-axis, namely: + − − + for the light rare-earth elements and + − + − for the heavy ones. A collinear magnetic order is

Table 4
The lattice parameters a, b and c, unit cell volume V and positional atoms parameters x_i, y_i, z_i for R_2TGe_6 (R = Pr, Nd, Tb, Gy, Ho, Er; T = Pd, Pt) obtained from the neutron diffraction data in the paramagnetic state.

	Pr_2PdGe_6	Nd_2PdGe_6	Tb_2PdGe_6	Dy_2PdGe_6	Ho_2PdGe_6	Tb_2PtGe_6	Er_2PtGe_6
T [K]	13.4 K	6.8 K	45 K	39.7 K	13 K	55.3 K	5.9 K
a [Å]	8.3278(16)	8.3099(12)	8.1861(18)	8.1604(16)	8.1502(13)	8.1383(11)	8.0925(16)
b [Å]	8.1717(15)	8.1588(12)	8.0548(16)	8.0363(14)	8.0371(12)	8.0475(10)	8.0193(16)
c [Å]	22.0606(39)	21.9964(31)	21.6022(50)	21.5331(44)	21.5006(37)	21.7086(27)	21.6146(44)
V [$Å^3$]	1501.28(48)	1491.33(37)	1424.39(53)	1412.13(48)	1408.38(39)	1421.77(31)	1402.71(48)
x(R)	0.2593(18)	0.2532(11)	0.2556(16)	0.2567(9)	0.2543(12)	0.2505(12)	0.2530(20)
y(R)	0.3960(23)	0.3823(20)	0.3810(46)	0.3748(17)	0.3785(40)	0.3829(43)	0.3678(30)
z(R)	0.0830(5)	0.0823(2)	0.0813(4)	0.0813(2)	0.0816(3)	0.0803(2)	0.0817(3)
y(T)	0.1393(26)	0.1343(27)	0.1499(35)	0.1702(33)	0.1472(27)	0.1283(18)	0.1292(26)
z(T)	0.1448(6)	0.1438(5)	0.1448(8)	0.1379(10)	0.1410(6)	0.1417(3)	0.14009(5)
x(Ge1)	0.2785(9)	0.2763(8)	0.2786(12)	0.2716(18)	0.2790(10)	0.2709(9)	0.2595(18)
y(Ge1)	0.1149(22)	0.11230(20)	0.1151(26)	0.1169(31)	0.1248(26)	0.1267(32)	0.1271(33)
z(Ge1)	0.1941(3)	0.1940(2)	0.1913(4)	0.1933(4)	0.1923(3)	0.1935(3)	0.1941(5)
y(Ge2)	0.1120(21)	0.1138(22)	0.1045(28)	0.0914(29)	0.1084(28)	0.1127(29)	0.0946(29)
z(Ge2)	0.4612(6)	0.4612(5)	0.4617(7)	0.4540(8)	0.4572(6)	0.4615(5)	0.4665(7)
y(Ge3)	0.1141(24)	0.1128(24)	0.1321(38)	0.1320(48)	0.1297(32)	0.1277(37)	0.1205(42)
z(Ge3)	0.0278(6)	0.0285(5)	0.0292(7)	0.0241(8)	0.0297(5)	0.0311(5)	0.0355(9)
y(Ge4)	0.3396(15)	0.3440(15)	0.3540(29)	0.3715(47)	0.3413(19)	0.3502(18)	0.3624(39)
z(Ge4)	0.3106(7)	0.3099(6)	0.3099(9)	0.3137(9)	0.3102(7)	0.3079(6)	0.3120(8)
y(Ge5)	0.3907(24)	0.3990(19)	0.4004(30)	0.4141(31)	0.4036(24)	0.4025(20)	0.4135(26)
z(Ge5)	0.2000(6)	0.1994(6)	0.1997(9)	0.2040(8)	0.1971(8)	0.1947(6)	0.1947(10)
R_{Bragg} [%]	6.67	5.59	8.80	7.56	6.22	4.91	9.21
R_{prof} [%]	5.27	3.39	4.61	2.34	2.70	2.72	5.14

Table 5
Sequence of the signs of the Fourier components of the magnetic structure as obtained from symmetry analysis performed for the **k** = [0, 0, 0] propagation vector and 16 g Wyckoff site. Only the basis vectors that fit the experimental data are listed. The full symmetry analysis can be found in Table 1 in Ref. [15]. The u parameter corresponds to the Fourier component along the a-axis and the v parameter to that along the b-axis. The atom positions S9-S16 are obtained from those of S1-S8 by applying the centering translation [½, ½, 0]. The magnetic moments at positions linked by the centering translation are always coupled ferromagnetically.

Atom position	Γ_3(u)	Γ_3(v)	Γ_8(v)	Γ_8(u)	Γ_6(u)
S1 (x, y, z)	+	+	+	+	+
S2(−x, −y+½, z+½)	−	−	+	+	+
S3 (−x, y+½, −z+½)	+	−	−	+	−
S4 (x, −y, −z)	−	+	−	+	−
S5 (−x, −y, −z)	+	+	−	−	−
S6 (x, y+½, −z+½)	−	−	−	−	−
S7 (x, −y+½, z+½)	+	−	+	−	+
S8 (−x, y, z)	−	+	+	−	+

observed for R = Nd and Er, and a non-collinear one for R = Pr, Tb, Dy, Ho. The non-collinear order is different from that observed in the R_2NiGe_6 compounds [12–15]. Another difference is detected between the magnetic structures of Nd_2NiGe_6 and Nd_2PdGe_6: in the first compound the magnetic order is stable in the entire temperature range up to the Néel temperature, while in the second one a change of the magnetic order from a collinear to a modulated one is observed at T = 4 K. This change results from the competition between the exchange interactions of RKKY-type and the influence of crystalline electric field (CEF) [25]. In R_2PdGe_6 (R = Tb-Ho) and Tb_2PtGe_6 a non-collinear AF ordering in the (0 0 1) plane with components along the a- and b-axes is observed. The magnetic moments form an angle φ with the b-axis equal to ~30° for Pr_2PdGe_6, ~15° for Tb_2TGe_6 and ~25° for Dy_2PdGe_6 and Ho_2PdGe_6. In Er_2PdGe_6 the magnetic moments are parallel to the a-axis as found previously in Er_2NiGe_6. A drastic change of the direction of magnetic moments between the Tb-, Dy-, Ho- and Er-based compounds is connected with the change of the sign of the Stevens operator α_J from negative (Tb, Dy, Ho) to positive (Er).

Fig. 8 shows the experimentally determined values of the Néel (T_N) and paramagnetic Curie (θ_p) temperatures for R_2TGe_6 (T = Ni, Pd) as a function of the de Gennes factor. The linear dependence, predicted by the RKKY theory, is represented by the solid lines which are normalized with respect to the data obtained by the respective Gd-based compounds. The theoretical de Gennes scaling is fulfilled for a majority of the investigated compounds, confirming the indirect exchange interactions of the RKKY-type. This result is in agreement with the large R-R interatomic distances and metallic character of the temperature dependence of the electrical resistivity [21]. Noticeable discrepancy between the experimental and theoretical values of T_N for Tb_2TGe_6 (T = Ni, Pd) can be attributed to the influence of the crystalline electric field [26]. The role of the CEF manifests itself also in a reduction of the magnetic moments in the ordered state in comparison to the free R^{3+} ion values (see Table 2).

The presented data are in agreement with the magnetic data collected for single crystals [21] indicating:

- a collinear AF ordering with the Gd moments along b-axis in Gd_2PdGe_6,
- the b-axis being a hard magnetic direction and the magnetic moments located in the a-b plane in Tb_2PdGe_6 (the results based on the temperature dependence of magnetoresistance).

Both the previously reported R_2TGe_6 (T = Ni, Cu; R = Tb, Ho and Er) [13] as well as the R_2PdGe_6 (R = Pr, Nd, Gd-Er) and R_2PtGe_6 (R = Tb, Ho, Er) presented in this work have an orthorhombic layered crystal structure which is related to the *Amm*2 space group for the first group of compounds and to *Cmca* for the second one. A change in the space group results in a doubling of the a and b lattice parameters for the second group as well as in a change of the local symmetry of the rare earth atoms. However, the macroscopic parameters, like the Néel and paramagnetic Curie temperatures, effective magnetic moments and critical magnetic fields are not much affected (compare the data in Table 1 in Ref. [13] to those in Table 2 in this work). On the contrary, the change in the local symmetry and the corresponding modification of the CEF parameters influences the microscopic magnetic order, i.e. collinear magnetic structures are favored in R_2TGe_6 (T = Ni, Cu; R = Tb, Ho and Er) [13] while non-collinear ones are favored in R_2PdGe_6 (R = Pr, Nd, Gd-Er) and R_2PtGe_6 (R = Tb, Ho, Er).

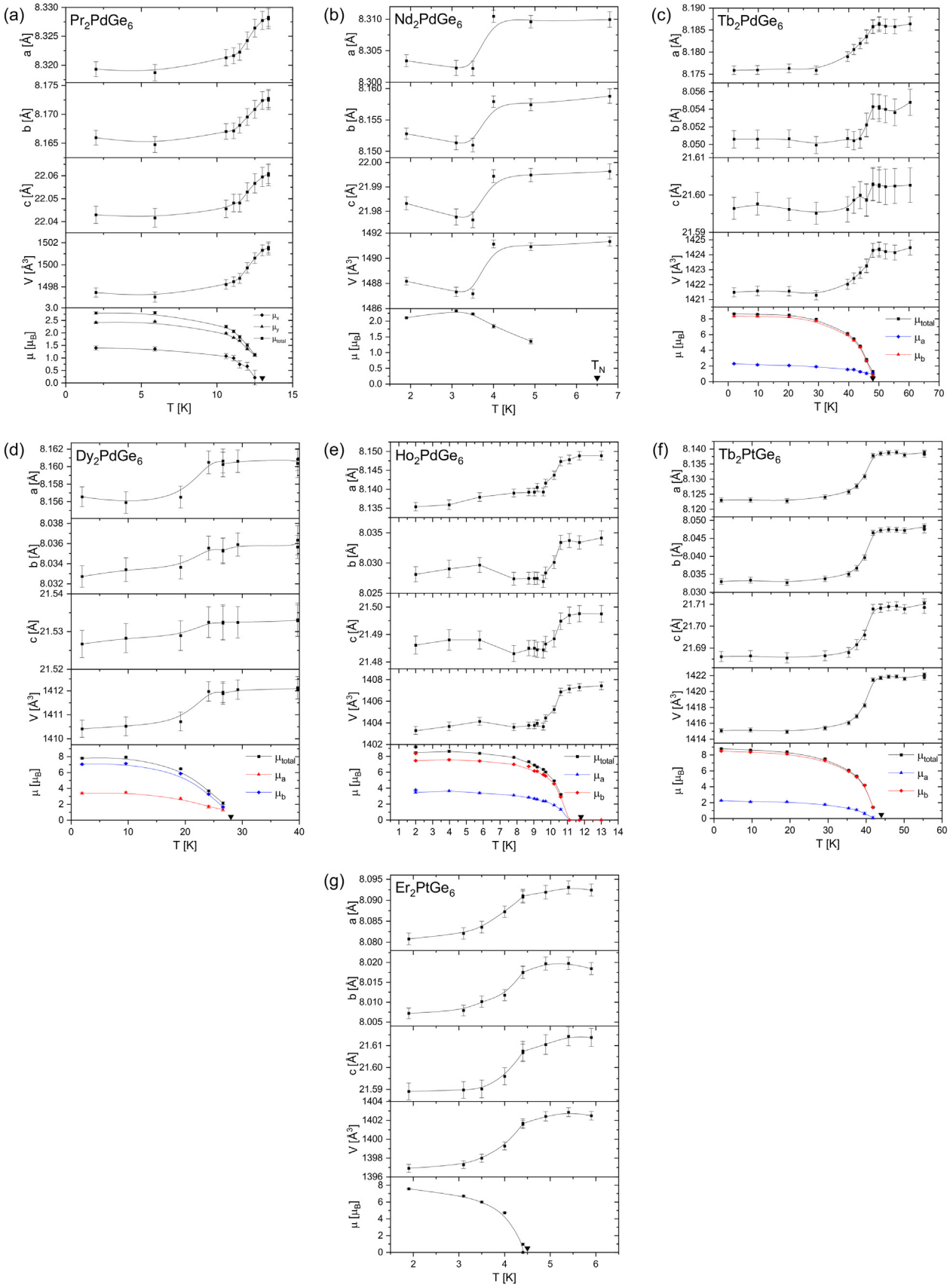

Fig. 7. Temperature dependence of the a, b and c lattice parameters together with the unit cell volume V and the values of the magnetic moments μ in a) Pr_2PdGe_6, b) Nd_2PdGe_6, c) Tb_2PdGe_6, d) Dy_2PdGe_6, e) Ho_2PdGe_6, f) Tb_2PtGe_6 and g) Er_2PtGe_6. The Néel temperature is marked by the black triangle at the bottom of each figure.

Table 6
Jump in the lattice parameters ($\Delta a = a_p - a_o$) and unit cell volumes ($\Delta V = V_p - V_o$) at the respective Néel temperatures for the R_2TGe_6 (T = Pd, Pt) compounds. o and p indicate the magnetically ordered and paramagnetic states, respectively, as derived from neutron diffraction. In the case of Nd_2PdGe_6, the data refer to the transition between the commensurate and incommensurate magnetic structures.

Compound	Δa [Å]	Δb [Å]	Δc [Å]	ΔV [Å^3]
Pr_2PdGe_6	0.0086	0.0072	0.018	4.22
Nd_2PdGe_6	0.008	0.0075	0.0188	3.88
Tb_2PdGe_6	0.010	0.0035	0.007	3.00
Dy_2PdGe_6	0.0045	0.002	0.003	1.30
Ho_2PdGe_6	0.0085	0.0075	0.03	4.13
Tb_2PtGe_6	0.015	0.0125	0.025	7.0
Er_2PtGe_6	0.011	0.011	0.025	5.6

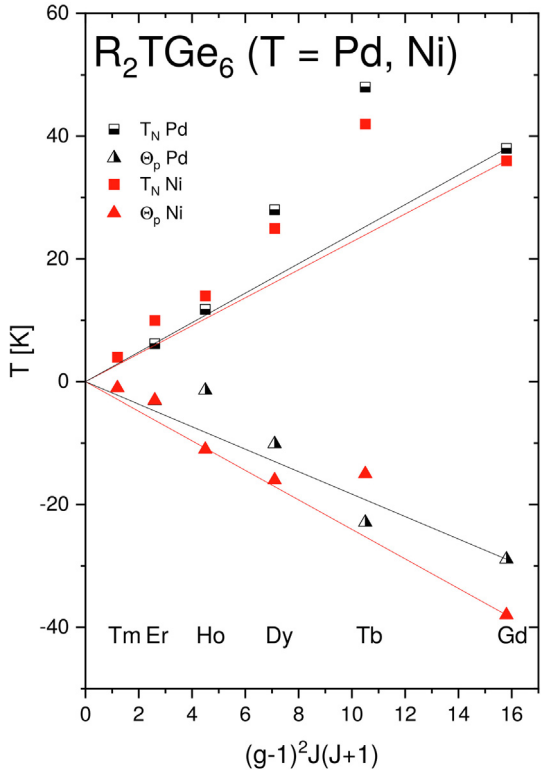

Fig. 8. The Néel and paramagnetic Curie temperatures vs. de Gennes factor $(g_J - 1)^2J(J + 1)$ for the R_2PdGe_6 and R_2NiGe_6 compounds. The solid lines represent the theoretical dependence predicted by the RKKY theory. The calculated values are normalized to the experimentally observed temperatures for the respective Gd-based compounds.

5. Summary

The results presented in this work confirm that the ternary R_2TGe_6 (R = Pr, Nd, Gd-Er; T = Pd, Pt) compounds crystallize in the orthorhombic Yb_2PdGe_6-type structure (space group *Cmca*). The magnetic and neutron diffraction data indicate that the magnetic properties in these compounds are derived from the well localized $4f^n$-electrons of the rare earth atoms. In all of the compounds the rare earth moments order antiferromagnetically at low temperatures and form collinear magnetic structures in Nd_2PdGe_6 and Er_2PtGe_6 and non-collinear ones in R_2PdGe_6 (R = Pr, Tb-Ho) and Tb_2PtGe_6. The observed magnetic structures result from a competition between the exchange interactions and crystalline electric field.

Declaration of interests

The authors declare that they have no known competing financial interests or personal relationships that could have appeared to influence the work reported in this paper.

CRediT authorship contribution statement

Bogusław Penc: Formal analysis, Visualization. **Stanisław Baran:** Formal analysis, Investigation, Writing - review & editing, Visualization. **Andreas Hoser:** Investigation. **Janusz Przewoźnik:** Formal analysis, Investigation, Formal analysis, Writing - original draft, Visualization. **Andrzej Szytuła:** Investigation, Writing - review & editing.

Acknowledgement

Kind hospitality and financial support extended to two of us (S. B. and A. S.) by the Helmholtz-Zentrum Berlin für Materialien und Energie (HZB) is gratefully acknowledged.

The research was partly carried out with the equipment purchased thanks to the financial support of the European Regional Development Fund in the framework of the Polish Innovation Economy Operational Program (contract no. POIG.02.01.00-12-023/08).

References

[1] M.B. Konyk, P.S. Salamakha, O.J. Bodak, V.K. Pecharsky, Kristallographia 33 (1988) 838–840.
[2] O. Sologub, K. Hiebl, P. Rogl, O. Bodak, J. Alloys Compd. 227 (1995) 37–39.
[3] M.L. Fornasini, P. Manfrinetti, P. Palenzona, Z. Kristallogr, NCS 217 (2002) 173–174.
[4] A. Gribanov, S. Safronov, E. Murashova, Y. Seropegin, J. Alloys Compd. 542 (2012) 28–31.
[5] D. Kaczorowski, A.V. Gribanov, P. Rogl, S.F. Dunaev, J. Alloys Compd. 685 (2016) 957–961.
[6] R. Wawryk, R. Troć, A.V. Gribanov, J. Alloys Compd. 520 (2012) 255–261.
[7] R. Freccero, P. Solokha, D.M. Proserpio, A. Saccone, S. De Negri, Dalton Trans. 46 (2017) 14021–14033.
[8] M. Konyk, L. Romaka, D. Gignoux, D. Fruchart, O. Bodak, Yu. Gorelenko, J. Alloys Compd. 398 (2005) 8–11.
[9] H. Yamamoto, I. Oguro, M. Ishikawa, J. Phys. Soc. Jpn. 65 (1996) 3464–3466.
[10] D.X. Li, S. Nimori, Y.X. Li, K. Koyama, Y. Shiokawa, J. Alloys Compd. 408–412 (2006) 122–126.
[11] D. Kaczorowski, M. Konyk, A. Szytula, L. Romaka, O. Bodak, Solid State Sci. 10 (2008) 1891–1894.
[12] B. Penc, A. Arulraj, S. Baran, N. Stusser, A. Szytula, Solid State Common. 142 (2007) 627–630.
[13] B. Penc, S. Baran, A. Hoser, A. Szytula, J. Alloys Compd. 803 (2019) 307–313.
[14] B. Penc, S. Baran, A. Hoser, A. Szytula, Phase Trans. 92 (2019) 1118–1126.
[15] J. Qi, W. Ren, C.-W. Wang, L. Zhang, Z. Zhang, J. Alloys Compd. 805 (2019) 1260–1265.
[16] M. Konyk, B. Kuzhel, Yu. Stadnik, Yu. Gorelenko, Ya. Mudryk, A. Waskiv, J. Alloys Compd. 459 (2008) 18–21.
[17] M.B. Konyk, L.P. Romaka, Yu.K. Gorelenko, O.I. Bodak, J. Alloys Compd. 311 (2000) 120–123.
[18] A.M. Strydom, A.V. Gribanov, Yu.D. Seropegin, R. Wawryk, R. Troc, J. Magn. Magn. Mater. 283 (2004) 181–189.
[19] Y.T. Fan, W.H. Lee, Y.Y. Chen, Phys. Rev. B 69 (2004) 132401.
[20] L. Zhang, W.-J. Ren, Z.-D. Zhang, J. Magn. Magn. Mater. 460 (2018) 239–242.
[21] L. Zhang, W. Ren, X. Luo, Z. Zhang, J. Mater. Sci. Technol. 35 (2019) 764–768.
[22] R. Troć, R. Wawryk, K. Gofryk, A.V. Gribanov, Y.D. Seropegin, J. Phys.: Condens. Matter 23 (2011) 146001.
[23] K. Shigetoh, D. Hirata, M.A. Avila, T. Takabatake, J. Alloys Compd. 403 (2005) 15–18.
[24] J. Rodriguez-Carvajal, Physica B 192 (1993) 55–69.
[25] D. Gignoux, D. Schmitt, Phys. Rev. B 48 (1993) 12682–12691.
[26] D.R. Noakes, G.K. Shenoy, Phys. Lett. 91A (1982) 35–36.